water

MDPI

Article

Characterization of the Adsorption of Cu (II) from Aqueous Solutions onto Pyrolytic Sludge-Derived Adsorbents

Minghui Wang [1,2], Tao Chen [3,*], Bo Yan [1,3], Lili Li [4], Damao Xu [1,2] and Xianming Xiao [1]

1 State Key Laboratory of Organic Geochemistry, Guangzhou Institute of Geochemistry, Chinese Academy of Sciences, Guangzhou 510640, China; 18371807641@163.com (M.W.); bo.yan@m.scnu.edu.cn (B.Y.); tchen259@163.com (D.X.); xmxiao@gig.ac.cn (X.X.)
2 University of Chinese Academy of Sciences, Beijing 100082, China
3 The Environmental Research Institute; MOE Key Laboratory of Theoretical Chemistry of Environment, South China Normal University, Guangzhou 510006, China
4 College of Environmental Science and Engineering, Zhongkai University of Agriculture and Engineering, Guangzhou 510000, China; lilili@gig.ac.cn
* Correspondence: tao.chen@m.scnu.edu.cn

Received: 22 November 2018; Accepted: 7 December 2018; Published: 10 December 2018

Abstract: The adsorption of Cu (II) onto two typical types of pyrolytic sludge was investigated in this study. The examined conditions include pH, adsorption time, and temperature, as well as the dosage of adsorbents. Results show that the adsorbents removed the Cu (II) effectively. The adsorbent made from pyrolyzed paper mill sludge (Cu_{MS}) exhibited exceptional performance, with a removal efficiency of around 100%. Moreover, the adsorption of Cu (II) onto Cu_{MS} was not affected by pH in the range of 3–9. The kinetic data showed better conformation with the pseudo-second-order kinetic model, and the adsorption processes of the Cu_{MS} fit well to the Langmuir isotherm model. The adsorption capacity reached 4.90 $mg \cdot g^{-1}$ under appropriate conditions. Microscopic analysis and FT-IR analysis revealed that the adsorbent with porous structure and high monosilicate content was beneficial to Cu (II) adsorption. Thus, the Cu_{MS} is a potentially promising candidate for retaining Cu (II) in aqueous environments.

Keywords: pyrolytic sewage sludge; adsorbent; Cu (II) adsorption characterizations

1. Introduction

There is steady concern about the pervasive detection of heavy metals in aquatic environments, as heavy metals are increasingly discharged into the drainage systems by the electroplating, metallurgical, paper manufacturing, and tannery industries. These elements are generally known to exhibit acute toxicity and inflict permanent damage on living organisms even at extremely low concentrations [1–3]. Hence, their sufficient removal and reclamation is pressing. Treatment technologies for water remediation, such as physical–chemical precipitation, membrane filtration, ion exchange, nanotechnology, and adsorption, have been well developed to eliminate the pollutants over the years [4]. Among these techniques, adsorption has been extensively used due to its unique properties, such as efficient performance, operational simplicity and economic feasibility [5,6]. In detail, the developed adsorbents have a relatively extraordinary capacity and large surface area, such that they can decrease the heavy metal concentrations to an acceptable level [7,8]. In view of the intended applications, the fabrication of adsorbent materials involves severe technological requirement limitations with respect to cost effectiveness, available precursors, applicable functions, and corrosion resistance. Therefore, the feasibility of this work has to be taken into account [9–11]. Sewage sludge,

generated as a by-product of the wastewater treatment process, can be converted to an attractive adsorbent [12]. The general adsorption performances of pyrolytic sludge are definitely far from meeting the needs of commercial applications. Pyrolytic sludge usually suffers from slow adsorption or limited adsorption capacity, probably due to the high ash content, which is inevitably produced during the pyrolytic process. However, resource utilization for sewage sludge will be a preferred and attractive application option in coming years [9]. In other words, it is imperative to redefine a sustainable destination for these engineered materials [6,13,14]. As confirmed in the literature, through oxygen-limited pyrolysis and chemical treatment, sewage sludge can be converted into cost-effective and eco-friendly adsorbents [15,16]. Compared to untreated sewage sludge, the leaching efficiency and mobility of heavy metals present in the pyrolytic sludge were dramatically reduced [17]. These innovative and promising adsorbent materials, featuring double benefits of favorable adsorption properties and renewable sources, were used as substitutes for activated carbon. Indeed, their particular properties are superior to those of activated carbon [18].

Herein, the straightforward objective of the present study was to describe the adsorption characteristics of pyrolytic sludge-based adsorbents with respect to Cu (II)-containing aqueous solutions. For comparison, two typical low-cost adsorbents derived from excess domestic sewage sludge (SS) and paper mill sludge (MS) were prepared by pyrolysis technology under laboratory conditions, and their underlying discrepancies in adsorption characterizations were fully revealed. To this end, simulated batch experiments at environmentally relevant concentrations were conducted to symmetrically investigate the effects of variable conditions on their removal efficiency and adsorption performance. Subsequently, the dominant mechanism for the adsorption was elucidated in detail based on the gathered results with high accuracy and reliability. Similar to qualitative indications reported previously, this study documents a favorable strategy bridging the gap between undesired waste utilization and intractable environmental repercussions.

2. Materials and Methods

2.1. Sludge Collection and Preparation

The original types of sewage sludge used in the carbonaceous absorbent preparation were respectively collected from a sewage treatment plant and a paper mill sewage treatment plant located in Guangzhou, South China. Sludge was immediately stored in a refrigerator (4 °C) before use. The sludge was air-dried at room temperature, ground into powder, and then sieved with the desired particle diameter ranging from 0.15 mm to 0.25 mm. The sludge was transported to porcelain crucibles and then pyrolyzed using a muffle furnace at 800 °C for 3 h (heating rate of 10 °C/min) under an inert atmosphere. Afterwards, the pyrolyzed sludge was naturally cooled to room temperature. The obtained samples were abbreviated as Cu_{SS} and Cu_{MS}, respectively, for sludge collected from the sewage treatment plant and the paper mill sewage treatment plant. After conversion, samples were repeatedly washed with distilled water to remove chemical residues remaining in the resultant product.

2.2. Batch Adsorption Experiments

The Cu (II) standard stock solutions were freshly prepared using $CuCl_2$, and the working solutions were obtained by successively diluting the stock solutions with distilled water. Simulated batch absorption experiments were performed in 250 mL Erlenmeyer flasks with stoppers. The pH of Cu (II)-bearing solutions was adjusted by adding 0.1 mol·L^{-1} HCl or NaOH solutions. A specific amount of the solid adsorbents was initially dispersed into 100 mL of a simulated solution of Cu (II) at defined concentrations. The homogeneous mixtures were then intensively shaken in the reciprocating water-bath oscillator operated at 220 rpm and three controlled temperatures (20, 30, and 40 °C). The suspension solution was collected for analysis at prescribed time intervals. Samples were centrifuged at 4000 rpm for 20 min, and then filtered with 0.45-μm membranes before analysis. The percentage removal efficiency (RE) of the experiments was estimated according to Equation (1).

In addition, the amount of Cu (II) adsorbed per unit mass of adsorbent (q_t, mg·g^{-1}) at time t (min) was calculated using Equation (2).

$$\mathrm{RE}(\%) = \frac{C_i - C_t}{C_i} \times 100\% \quad (1)$$

$$q_t = \frac{(C_i - C_t) \times V}{M} \quad (2)$$

where C_i (mg·L^{-1}) and C_t (mg·L^{-1}) are the initial concentration and the residual concentration of Cu (II), respectively; V (L) is the volume of Cu (II) solution; and M (g) represents the mass weight of adsorbents.

2.3. Analytical Methods and Characterization

Concentrations of metals were determined by flame atomic absorption spectrometry (AAS, ZA-3000, Hitachi, Toyota, Japan). The metal-leaching characteristics were obtained according to the Chinese standard method (HJ/T299-2007). The chemical composition was determined by X-ray fluorescence spectroscopy (XRF1800, Shimadzu, Kyoto, Japan). All solution pH values were monitored using a digital pH meter (pH-3C, Leici, Shanghai, China). The surface morphology was examined by scanning electron microscopy (SEM, S-4800, Hitachi, Toyota, Japan). The surface area and porosity were measured using an ASAP 2020 Surface Area and Porosity Analyzer (Micromeritics, Washington, WA, USA). Fourier Transform infrared spectroscopy (FT-IR) was obtained using a Bruker VERTEX 70 Fourier transform infrared spectrometer (Bruker, Billerica, German) with the KBr pressed pellet method.

3. Results and Analysis

3.1. Physical and Chemical Properties and Leaching Toxicity Characteristics of Adsorbents

The chemical compositions were summarized in Table 1. The chemical compositions in Cu_{SS} were mainly Al_2O_3, P_2O_5 and SiO_2, while the major chemical constituents in Cu_{MS} were Al_2O_3, CaO, and SiO_2.

Table 1. Chemical composition of the Cu_{SS} and Cu_{MS} used in the present study. Cu_{SS}: the adsorbent made from the sewage sludge; Cu_{MS}, the adsorbent made from pyrolyzed paper mill sludge.

Chemical Composition	Al_2O_3	CaO	Fe_2O_3	K_2O	MgO	MnO	Na_2O	P_2O_5	SiO_2	TiO_2
Cu_{SS} (wt %)	18.41	3.59	7.97	3.93	2.72	0.06	0.78	10.42	51.22	0.92
Cu_{MS} (wt %)	15.95	50.34	0.84	0.35	2.17	0.03	0.42	0.96	28.41	1.03

The total and leaching concentrations of heavy metals in Cu_{SS} and Cu_{MS} are presented in Table 2. In this study, the threshold values in the standards (GB4284-84 and GB5085.3-2007) promulgated by the Chinese Ministry of Ecology and Environment (CMEE) were adopted. The total and leaching metal concentrations were lower than the permissible limits. Accordingly, Cu_{SS} and Cu_{MS} could be further applied for the treatment of waste water.

Table 2. Total and leaching concentrations of heavy metals in Cu_{SS} and Cu_{MS}.

Materials		Heavy Metals					
		Cr	Ni	Cu	Pb	Mn	Zn
Cu_{SS}	total contents (mg kg^{-1})	49.6	74.0	190	82.4	214	909
	leaching concentration (mg L^{-1})	8.19	4.10	5.69	ND [1]	10.1	1.27
Cu_{MS}	total contents (mg kg^{-1})	19.4	103	175	ND	161	717
	leaching concentration (mg L^{-1})	1.32	3.30	6.41	ND	7.40	3.89

Table 2. *Cont.*

Materials		Heavy Metals					
		Cr	Ni	Cu	Pb	Mn	Zn
Threshold values for total contents [2]	pH ≥ 6.5 (mg kg^{-1})	1000	200	500	1000	NA	1000
	pH < 6.5 (mg kg^{-1})	600	100	250	300	NA	500
Permissible limits for leaching toxicity [3] (mg kg^{-1})		15.0	5.00	100	5.00	NA	100

[1] Not detected; [2] The threshold values of the Chinese control standards for pollutants in sludge from agricultural use (GB4284-84); [3] The permissible limits of the Chinese control standards for identification standard of hazardous wastes-identification of extraction toxicity (GB5085.3-2007).

3.2. Effect of pH on Adsorption

The pH of a solution plays an important role in the adsorption process and can radically change the existing speciation of an adsorbate and surface charge of an adsorbent [19]. In the present study, the effect of pH was tested under a temperature of 25 °C, an initial Cu(II) concentration of 25 mg·L^{-1}, a reaction time of 360 min, and dosages of Cu_{SS} and Cu_{MS} of 20 g·L^{-1} and 5 g·L^{-1} respectively, depending on their adsorption capacity.

According to Figure 1, by increasing the $pH_{initial}$ from 3 to 7, the RE of Cu_{SS} sharply increased from 21.56 to 73.60%. When the $pH_{initial}$ was 8, the RE and q_t reached the maximum values of 77.12% and 0.964 mg·g^{-1}, respectively. Interestingly, when the $pH_{initial}$ increased from 6 to 7, the RE was drastically increased from 52.84% to 73.60%. It can be concluded that Cu (II) competed with H^+ for the vacant binding sites in Cu_{SS} under acidic conditions. In contrast, Cu (II) adsorption of Cu_{MS} was less affected by pH, and its RE and q_t values were greater than 96.81% and 4.84 mg·g^{-1}, respectively.

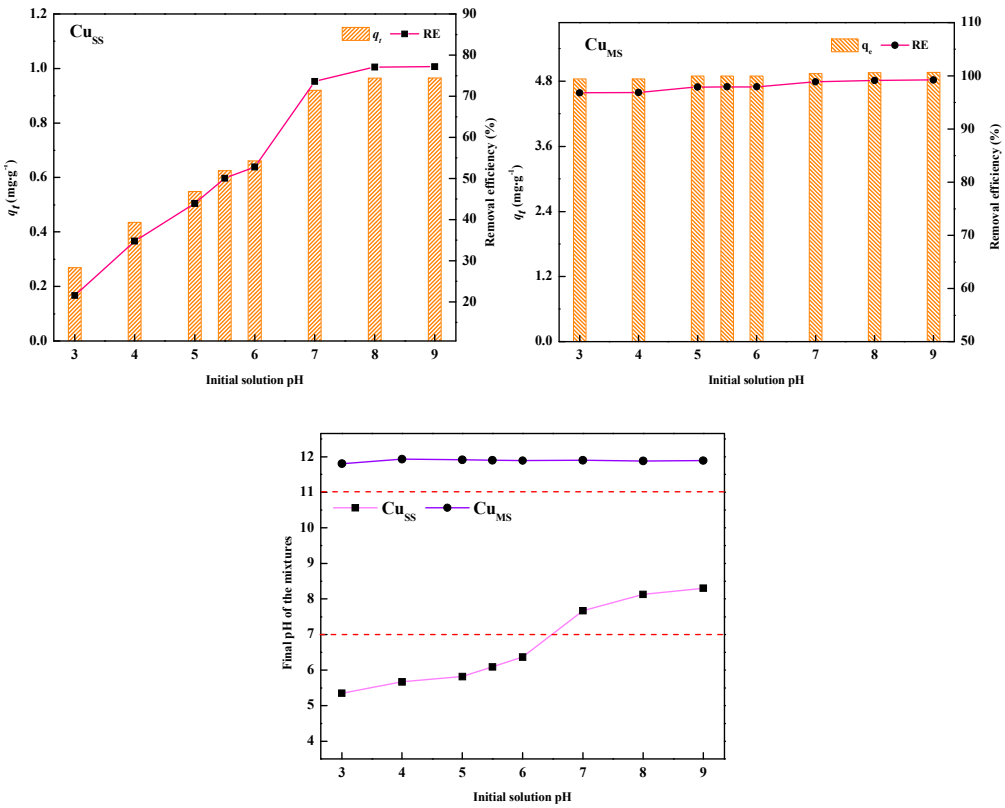

Figure 1. Effect of solution $pH_{initial}$ on the Cu (II) removal of the adsorbents. $pH_{initial}$: initial pH value of the solution.

As shown in Figure 1, the solution pH_{final} in mixtures with Cu_{SS} increased from 5.14 to 8.30. The reason behind this pattern was that the hydrolysis of Cu (II) varied dramatically from weak to

strong with the solution pH ranging from acidic to alkaline conditions. Additionally, compared with Cu_{SS}, Cu_{SS} had notably stronger buffering ability by releasing reactive OH groups into mixtures, with the adsorption of Cu (II) by Cu_{MS}.

3.3. Effect of Constant Temperature on Adsorption

The effect of the temperature was also investigated, under conditions of pH = 7, Cu(II) concentration of 25 mg·L^{-1}, and dosages of Cu_{SS} and Cu_{MS} of 20 g·L^{-1} and 5 g·L^{-1}, respectively. According to Figure 2, when the temperature increased from 20 to 40 °C, the RE and adsorption capacity of Cu_{SS} considerably increased. This implied that the adsorption behavior was an endothermic process in nature, showing an enhanced adsorption capacity at higher temperatures. And the higher of the temperature, the faster the equilibrium of adsorption reached. However, the adsorption process of Cu_{MS} was not affected by the temperature, especially when the temperature reached 30 °C.

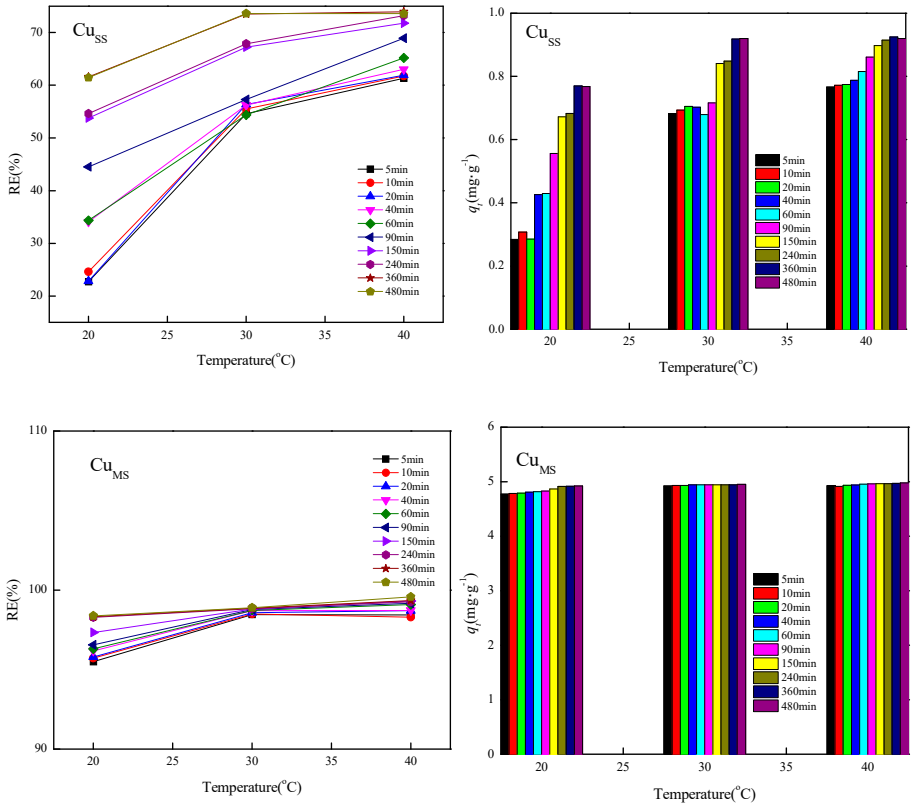

Figure 2. Effect of temperatures and time on Cu(II) adsorption by Cu_{SS} and Cu_{MS}.

3.4. Effect of Adsorption Dosage on Adsorption

As shown in Figure 3, when the dosages increased from 1 to 20 g·L^{-1}, the RE of Cu_{SS} almost reached a balance, increasing from 44.82 to 73.60%. The q_t decreased with the ascending dosage of the Cu_{SS}, and it was affected by the reaction time. The maximum q_t for Cu_{SS} was 2.02 mg·g^{-1} when the dosage was 5 g·L^{-1} after the 480-min adsorption process.

When the dosages of Cu_{MS} ranged from 1 to 5 g·L^{-1}, the RE of Cu_{MS} reached a balance, and it reached approximately 100%. Interestingly, the reaction time had little effect on RE and the q_t value. These results indicated that, in comparison with Cu_{SS}, Cu_{MS} showed a lower dosage and a higher adsorption capacity.

A pseudo-second-order model is commonly employed for the adsorption mechanism, where the main interaction involved in adsorption was adsorbent-adsorbate affinities in an aqueous

solution. In an attempt to discriminate the adsorption behavior, the kinetics data were fitted to a pseudo-second-order model, as empirically expressed mathematically in Equation (3) [3,20,21].

$$\frac{t}{q_t} = \frac{1}{k_2 \times q_e^2} + \frac{t}{q_e} = \frac{1}{h_0} + \frac{t}{q_e} \tag{3}$$

where k_2 is the second-order rate constants for the adsorption process, g·mg^{-1}·min^{-1}; t is the reaction time, min; q_e is the equilibrium adsorption capacity amount of the adsorbent, mg·g^{-1}; and h_o represents the initial adsorption rate, mg·g^{-1}·min^{-1}.

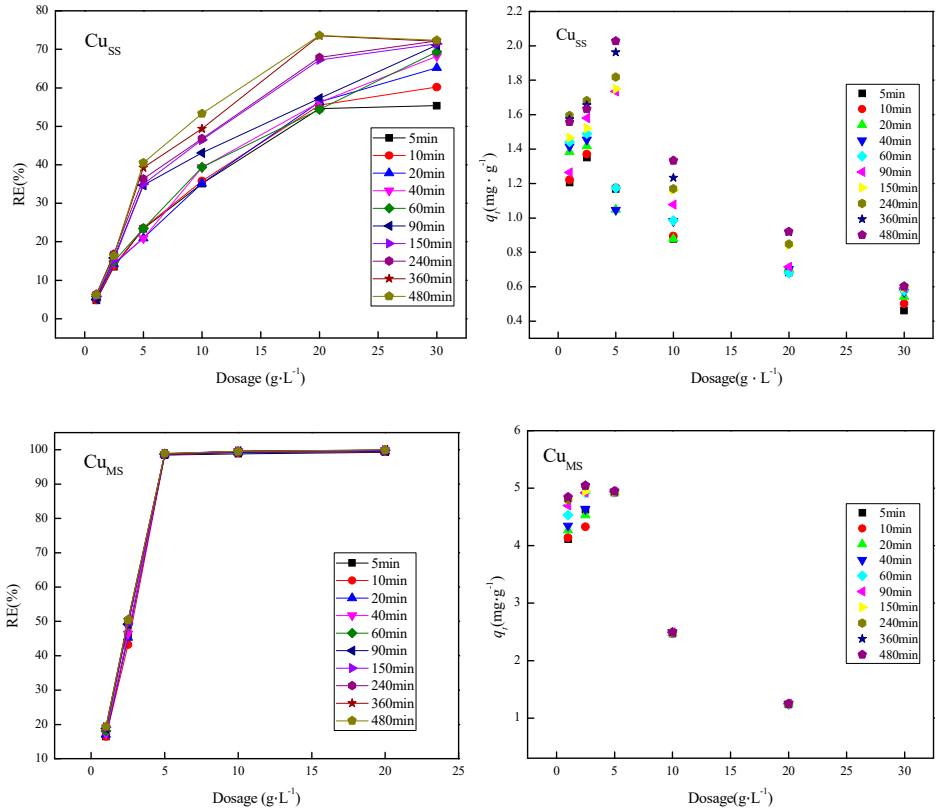

Figure 3. The effect of dosage on the Cu (II) adsorption (temperature is 25 °C, Cu(II) is 25 mg·L^{-1}; pH is 7).

The fitted curves of the pseudo-second-order kinetic model for Cu (II) onto Cu$_{SS}$ and Cu$_{MS}$ at different doses and constant temperatures are depicted in Figure 4. Obviously, the model for the modified adsorbents at different doses were well fitted, the R^2 were higher than 0.99.

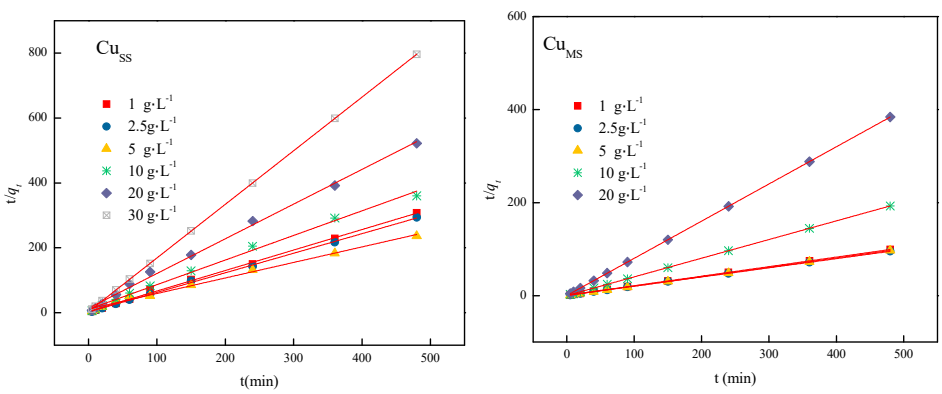

Figure 4. The pseudo-second-order model for the adsorption process.

The slope ($1/q_e$) and intercept (h_o, $1/(k_2 \times q_e^2)$), referring to the fitting values of the corresponding parameters, were determined by the linear plots t/q_t against t for the experimental data (Table 3). The second-order rate constants (k_2) and the initial adsorption rate (h_0) increased with increased adsorbent dosages. At the given experimental conditions, Cu_{MS} required less time to reach equilibrium than Cu_{SS}, likely because the q_e for Cu_{MS} was 2.5 times that for Cu_{SS}.

Table 3. Adsorption kinetics parameters for Cu (II) adsorption at different dosages.

	Dosage	Temperature	Pseudo-Second-Order Model	R^2	$1/q_e$	q_e	$1/(k_2 \times q_e^2)$	k_2
Cu_{SS}	1 g·L^{-1}	30 °C	y = 0.6267x + 4.2587	0.9964	0.6032	1.6578	2.4939	0.1459
	2.5 g·L^{-1}	30 °C	y = 0.6032x + 2.4939	0.9992	0.6032	1.6578	2.4939	0.1459
	5 g·L^{-1}	30 °C	Y = 0.4787x + 11.448	0.9929	0.4787	2.0890	11.4480	0.0200
	10 g·L^{-1}	30 °C	Y = 0.7584x + 10.749	0.9954	0.7584	1.3186	10.7490	0.0535
	20 g·L^{-1}	30 °C	y = 1.0694x + 14.01	0.9968	1.0694	0.9351	14.0100	0.0816
	30 g·L^{-1}	30 °C	y = 1.6519x + 3.6656	1.0000	1.6519	0.6054	3.6656	0.7444
Cu_{MS}	1 g·L^{-1}	30 °C	y = 0.2054x + 0.6007	0.9999	0.2054	4.8685	0.6007	0.0702
	2.5 g·L^{-1}	30 °C	y = 0.1973x + 0.4399	1.0000	0.1973	5.0684	0.4399	0.0885
	5 g·L^{-1}	30 °C	y = 0.2021x + 0.0228	1.0000	0.2021	4.9480	0.0228	1.7914
	10 g·L^{-1}	30 °C	y = 0.4016x + 0.0116	1.0000	0.4016	2.4900	0.0116	13.9037
	20 g·L^{-1}	30 °C	y = 0.7999x + 0.0403	1.0000	0.7999	1.2502	0.0403	15.8769

The Langmuir and Freundlich isotherm models were used to analyze the adsorption isotherms according to the data from Figure 3. The Langmuir isotherm model is expressed as Equation (4), and its linear form is expressed as Equation (5) [12].

$$q_t = \frac{K_L \times q_{max} \times C_e}{1 + K_L \times C_e} \tag{4}$$

$$\frac{C_e}{q_t} = \frac{1}{K_L \times q_{max}} + \frac{C_e}{q_{max}} \tag{5}$$

where K_L is the Langmuir adsorption constant related to adsorption energy and the affinity of binding sites; C_e is the equilibrium concentration in the solution, mg L^{-1}; and q_{max} is the maximum adsorption capacity of MS_x, mg g^{-1}.

The Freundlich isotherm model assumes that all adsorption sites in the MS_x are heterogeneous and that the adsorption mechanism is multilayer adsorption. The Freundlich isotherm model is expressed as Equation (6):

$$q_t = K_F \times C_e^{1/n} \tag{6}$$

where n is the heterogeneity factor and K_F is the Freundlich constant (mg g^{-1}). The linear form of the Freundlich equation is expressed as Equation (7):

$$\ln q_t = \ln K_F + \frac{1}{n} \ln C_e \tag{7}$$

The n is related to the adsorption intensity or surface heterogeneity. A lower value of n indicates a lesser heterogeneity. All of the thermodynamic parameters for the Langmuir model and Freundlich model are shown in Table 4. The adsorption of Cu_{MS} fitted well with the Langmuir isotherm model. The correlation coefficient values (R^2) for the Langmuir model were greater than 0.99. However, the adsorption of Cu_{SS} fitted badly both with the Langmuir isotherm model and the Freundlich model. The maximum adsorption capacity (q_{max}) of Cu_{MS} was 4.90 mg g^{-1}, and K_L for Cu_{MS} was 111.93 L g^{-1}, indicating that the Cu_{MS} had a strong adsorption capacity.

Table 4. Thermodynamic parameters for the Langmuir and Freundlich models.

Adsorbents	Langmuir Model			Freundlich Model		
	R^2	q_{max}	K_L	R^2	n	K_F
Cu_{SS}	0.4796	3.179	0.052	0.6750	1.479	0.23
Cu_{MS}	0.9994	4.901	111.93	0.6749	5.963	3.48

4. Discussion

As the adsorption tests and the analysis show, the pseudo-second-order kinetic model for Cu (II) onto the two adsorbents at different doses and temperatures were well fitted, the R^2 were higher than 0.99. However, Cu_{MS} required less time to reach equilibrium compared to Cu_{SS}, and the q_e for Cu_{MS} was about 2.5 times that for Cu_{SS}. Furthermore, the adsorption of Cu_{MS} was fitted well by the Langmuir isotherm model. The maximum adsorption capacity (q_{max}) of Cu_{MS} was 4.90 mg g^{-1}. The value was competitive with some similar low-cost adsorbents, including sawdust [22], coal [23], and also modified waste [24], their adsorption capacity was between 1.62 and 2.10 mg g^{-1}.

The micro-structural properties of Cu_{SS} and Cu_{MS} are illustrated in Figure 5. Both Cu_{SS} and Cu_{MS} exhibited irregular particles. More specifically, Cu_{SS} bears clearly large irregular agglomerates (Figure 5), whereas Cu_{MS} showed porous surface features, which could be beneficial for increasing its specific surface area and providing available active adsorption sites.

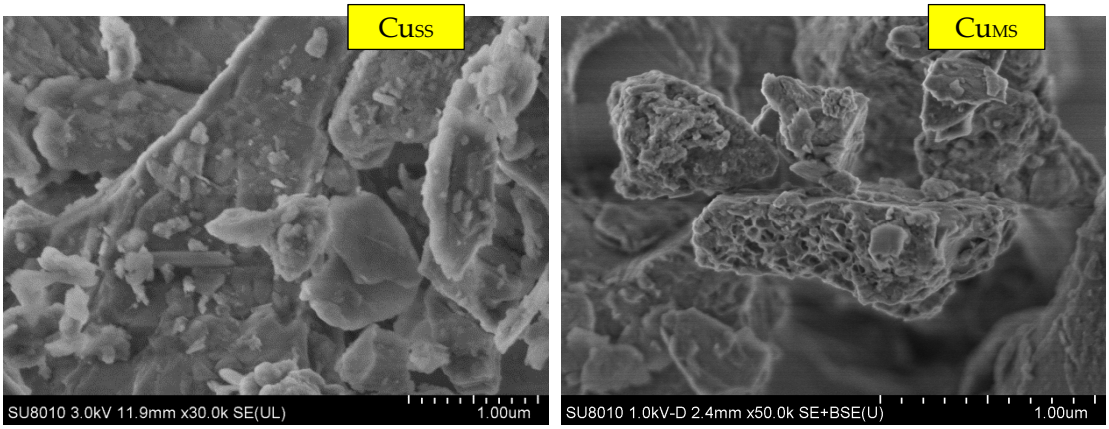

Figure 5. Representative SEM images of Cu_{SS} and Cu_{MS}.

With the characterization of surface area and porosity, it can be found that the BET-specific surface area of Cu_{MS} reached 386.22 $m^2 \cdot g^{-1}$, which was approximately 2 times greater than that of Cu_{SS} (115.31 $m^2 \cdot g^{-1}$). Furthermore, the micro-pore volume of Cu_{MS} reached 0.6893 $cm^3 \cdot g^{-1}$, which was approximately 2 times higher than that of Cu_{SS} (0.2653 $cm^3 \cdot g^{-1}$).

Additionally, compared with Cu_{SS}, Cu_{MS} had notably stronger buffering ability. With the chemical compositions analysis, we found that the major chemical constituents in Cu_{SS} were Al_2O_3, P_2O_5, and SiO_2, while the major chemical constituents in Cu_{MS} were Al_2O_3, CaO, and SiO_2. Thus, the mechanism for the adsorbents must be different.

FT-IR analysis of adsorbents after Cu(II) adsorption was conducted (Figure 6). The broad absorption band at 3423 cm^{-1} present in Cu_{SS} is ascribed to the −OH stretching vibrations [25]. The absorption band at 1051 cm^{-1} is ascribed to the stretching vibration of O-H. It can be deduced that the adsorption of Cu(II) on Cu_{SS} occurred and the H-bond and electrostatic interactions played an important role.

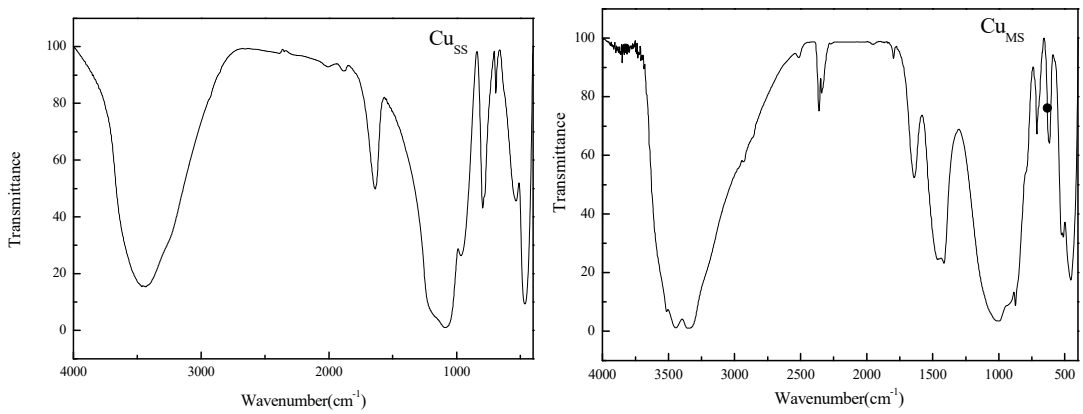

Figure 6. FT-IR spectra of adsorbents.

The absorption bands at 1090 and 1500 cm^{-1} are related to the Si−O−Si stretching vibrations, while the absorption band at 468 cm^{-1} is related to the Si−O bending vibrations [25], which is related to the disordering of SiO_4 [26], that is, a monosilicate is produced. The disordering of silicate in Cu_{MS} causes the overlap of the different absorption bands, which broaden the absorption band. Furthermore, the adsorption of the Cu would promote by the monosilicate [27].

5. Conclusions

Two types of pyrolytic sludge were studied for Cu(II) removal in this paper. Cu(II) adsorption by Cu_{MS} was not affected in the pH range of 3–9, whereas the pH values were narrow for Cu_{SS} adsorption of Cu(II). The adsorption residence time exerted insignificant impacts on the adsorption of Cu_{MS}, which was closely related to the dosage added. The maximum adsorption capacity of Cu_{MS} reached 4.90 mg/g. Moreover, the adsorption of the Cu_{MS} fitted well with the Langmuir isotherm model, and the pseudo-second-order kinetic model for Cu(II) onto the two adsorbents at different doses was also well fitted. Combining the surface area and porosity analysis and the FT-IR analysis, the higher adsorption capacity and the wider range of pH adaptation were due to its porous structure and higher monosilicate contents.

Author Contributions: Conceptualization, M.W. and T.C.; Writing—Original Draft Preparation, M.W. and X.X.; Writing—Review and Editing, T.C., B.Y., and X.X.; Project Administration, B.Y.; Methodology, B.Y. and L.L.; Data Curation, D.X.

Funding: This work was funded by the National Natural Science Foundation of China Youth Fund (No. 41503116), the Guangzhou Science and Technology Program (No. 201607020003), the Guangdong provincial science and technology program (No. 2014B090901040, 2015B020237003), and the Guangdong Natural Science Foundation (No. 2017A03031D05).

Conflicts of Interest: The authors declare no conflict of interest.

References

1. Björklund, K.; Li, L.Y. Adsorption of organic stormwater pollutants onto activated carbon from sewage sludge. *J. Environ Manag.* **2017**, *197*, 490–497. [CrossRef] [PubMed]
2. Monárrez-Cordero, B.E.; Amézaga-Madrid, P.; Fuentes-Cobas, L.; Montero-Cabrera, M.E.; Miki-Yoshida, M. High and fast adsorption efficiency of simultaneous As+3, As+5, and F-, by Al-doped magnetite synthesized *via* AACVD. *J. Alloys Compd.* **2017**, *718*, 414–424. [CrossRef]
3. Zhu, M.; Li, Z.; Wang, J.; Yue, T.; Li, R.; Li, Z. Adsorption of Cd (II) and Pb (II) by *in situ*, oxidized Fe_3O_4, membrane grafted on 316L porous stainless steel filter tube and its potential application for drinking water treatment. *J. Environ Manag.* **2017**, *196*, 127–136. [CrossRef]
4. Nielsen, L.; Zhang, P.; Bandosz, T.J. Adsorption of carbamazepine on sludge/fish waste derived adsorbents: Effect of surface chemistry and texture. *Biochem. Eng. J.* **2015**, *267*, 170–181. [CrossRef]

5. Podstawczyk, D.; Witek-Krowiak, A.; Dawiec-Liśniewska, A.; Chrobot, P.; Skrzypczak, D. Removal of ammonium and orthophosphates from reject water generated during dewatering of digested sewage sludge in municipal wastewater treatment plant using adsorption and membrane contactor system. *J. Clean. Prod.* **2017**, *161*, 277–287. [CrossRef]
6. Sanganyado, E.; Fu, Q.; Gan, J. Enantiomeric selectivity in adsorption of chiral β-blockers on sludge. *Environ. Pollut.* **2016**, *214*, 787–794. [CrossRef] [PubMed]
7. Xie, W.M.; Zhou, F.P.; Bi, X.L.; Chen, D.D.; Li, J.; Sun, S.Y.; Chen, X.Q. Accelerated crystallization of magnetic 4A-zeolite synthesized from red mud for application in removal of mixed heavy metal ions. *J. Hazard. Mater.* **2018**, *358*, 441–449. [CrossRef]
8. Wei, L.; Yang, L.; Noguera, D.R.; Zhao, N.; Yue, S.; Jing, D.; Zhao, Q.; Cui, F. Adsorption of Cu^{2+}, and Zn^{2+}, by extracellular polymeric substances (EPS) in different sludges: Effect of EPS fractional polarity on binding mechanism. *J. Hazard. Mater.* **2017**, *321*, 473–483. [CrossRef]
9. Liu, J.Y.; Ning, X.N.; Yang, Z.Y. Study of adsorbent derived from sewage sludge incineration residue for the removal of Ni^{2+} in wastewater. *Key Eng. Mater.* **2011**, *474–476*, 158–161. [CrossRef]
10. Pei, Y.Y.; Liu, J.Y. Adsorption of Pb^{2+} in wastewater using adsorbent derived from grapefruit peel. *Adv. Compos. Mater. Res.* **2011**, *391–392*, 968–972. [CrossRef]
11. Ferreira, C.I.; Calisto, V.; Otero, M.; Nadais, H.; Esteves, V.I. Removal of tricaine methanesulfonate from aquaculture wastewater by adsorption onto pyrolysed paper mill sludge. *Chemosphere* **2017**, *168*, 139–146. [CrossRef]
12. Rashed, M.N.; El-Daim, M.A.; Taher, E.; Fadlalla, S.M.M. Adsorption of methylene blue using modified adsorbents from drinking water treatment sludge. *Water Sci. Technol.* **2016**, *74*, 1885–1898. [CrossRef] [PubMed]
13. Orlandi, G.; Cavasotto, J.; Jr, M.F.; Colpani, G.L.; Magro, J.D.; Dalcanton, F.; Mello, J.M.; Fiori, M.A. An adsorbent with a high adsorption capacity obtained from the cellulose sludge of industrial residues. *Chemosphere* **2017**, *169*, 171–180. [CrossRef] [PubMed]
14. Silva, T.L.; Ronix, A.; Pezoti, O.; Souza, L.S.; Leandro, P.K.T.; Bedin, K.C.; Beltrame, K.K.; Cazetta, A.L.; Almeida, V.C. Mesoporous activated carbon from industrial laundry sewage sludge: Adsorption studies of reactive dye Remazol Brilliant Blue R. *Chem. Eng. J.* **2016**, *303*, 467–476. [CrossRef]
15. Jaria, G.; Calisto, V.; Gil, M.V.; Otero, M.; Esteves, V.I. Removal of fluoxetine from water by adsorbent materials produced from paper mill sludge. *J. Colloid Interface Sci.* **2015**, *448*, 32–40. [CrossRef]
16. Zielińska, A.; Oleszczuk, P. Evaluation of sewage sludge and slow pyrolyzed sewage sludge-derived biochar for adsorption of phenanthrene and pyrene. *Bioresour. Technol.* **2015**, *192*, 618–626. [CrossRef] [PubMed]
17. Hossain, M.K.; Strezov, V.; Chan, K.Y.; Nelson, P.F. Agronomic properties of wastewater sludge biochar and bioavailability of metals in production of cherry tomato (Lycopersicon esculentum). *Chemosphere* **2010**, *78*, 1167–1171. [CrossRef] [PubMed]
18. Devi, P.; Saroha, A.K. Simultaneous adsorption and dechlorination of pentachlorophenol from effluent by Ni-ZVI magnetic biochar composites synthesized from paper mill sludge. *Chem. Eng. J.* **2015**, *271*, 195–203. [CrossRef]
19. Kumar, A.S.K.; Jiang, S.J. Synthesis of magnetically separable and recyclable magnetic nanoparticles decorated with β-cyclodextrin functionalized graphene oxide an excellent adsorption of As (V)/(III). *J. Mol. Liq.* **2017**, *237*, 387–401. [CrossRef]
20. Chaudhry, S.A.; Zaidi, Z.; Siddiqui, S.I. Isotherm, kinetic and thermodynamics of arsenic adsorption onto Iron-Zirconium Binary Oxide-Coated Sand (IZBOCS): Modelling and process optimization. *J. Mol. Liq.* **2017**, *229*, 230–240. [CrossRef]
21. Zhang, X.; Gu, P.; Li, X.; Zhang, G. Efficient adsorption of radioactive iodide ion from simulated wastewater by nano Cu_2O/Cu modified activated carbon. *Chem. Eng. J.* **2017**, *322*, 129–139. [CrossRef]
22. Yu, B.; Zhang, Y.; Shukla, A.; Shukla, S.S.; Dorris, K.L. The removal of heavy metal from aqueous solutions by sawdust adsorption—removal of copper. *J. Hazard. Mater.* **2000**, *80*, 33–42. [CrossRef]
23. Karabulut, S.; Karabakan, A.; Denizli, A.; Yürüm, Y. Batch removal of copper(II) and zinc(II) from aqueous solutions with low-rank Turkish coals. *Sep. Purif. Technol.* **2000**, *18*, 177–184. [CrossRef]
24. Haoutia, R.E.; Anfara, Z.; Chennaha, A.; Amaterz, E.; Zbair, M.; Alem, N.E.; Benlhachemi, A.; Ezahria, M. Synthesis of sustainable mesoporous treated fish waste as adsorbent for copper removal. *Groundwater Sustain. Dev.* **2019**, *8*, 1–9. [CrossRef]

25. Shim, J.; Shea, P.J.; Oh, B.T. Stabilization of heavy metals in mining site soil with silica extracted from corn cob. *Water Air Soil Pollut.* **2014**, *225*, 1–12. [CrossRef]
26. Gyollai, I.; Krebsz, M.; Kereszturi, Á.; Bérczi, S.; Gucsik, A. FTIR-ATR spectroscopy of shock vein in mócs L6 chondrite. *J. Geophys. Res.* **2010**, *116*, 27–36.
27. Lei, C.; Yan, B.; Chen, T.; Xiao, XM. Preparation and adsorption characteristics for heavy metals of active silicon adsorbent from leaching residue of lead-zinc tailings. *Environ. Sci. Pollut. Res.* **2018**, *25*, 21233–21242. [CrossRef]